https://doi.org/10.5194/essd-2026-712
Preprint. Discussion started: 21 September 2026

Open Access Earth System Science Data Discussions

SDUST2025_SWOT: Global marine deflection of the vertical and gravity anomaly datasets derived from SWOT/KaRIn wide-swath altimetry using local geoid fitting

Huiying Zhang [1], Jinyun Guo [1*], Shaoshuai Ya [1], Shaofeng Bian [2], Yongjun Jia [3], Xin Liu [1]

1 College of Geodesy and Geomatics, Shandong University of Science and Technology, Qingdao 266590, China

2 Key Laboratory of Geological Survey and Evaluation of Ministry of Education, China University of Geosciences Wuhan, Wuhan 430074, China

3 National Satellite Ocean Application Service, Beijing 100081, China

Corresponding Author: Jinyun Guo, Email: jinyunguo1@126.com

Abstract. Satellite altimetry provides an important data source for recovering the marine gravity field. However, the conventional remove-compute-restore (RCR) strategy commonly used for deriving marine deflection of the vertical (DOV) causes the long-wavelength components of the derived DOV to depend to some extent on reference gravity field models. The two-dimensional (2D) sea surface height observations from SWOT/KaRIn wide-swath altimetry provide a new opportunity for constructing marine DOV datasets without relying on the conventional RCR strategy. Here, we construct a global 1′ × 1′ marine DOV dataset, named SDUST2025DOV_SWOT, based on multi-cycle SWOT/KaRIn wide-swath altimetry observations and a local geoid fitting approach. Based on SDUST2025DOV_SWOT, the corresponding marine gravity anomaly dataset SDUST2025GRA_SWOT is further derived. The datasets cover global ocean regions between 77.6°S and 77.6°N. The quality of the datasets is evaluated through comparisons with existing global products, including SIO V33.1DOV/GRA, SWOT_04DOV/GRA, and DTU21GRA, as well as independent shipborne gravity observations. The results show that SDUST2025DOV_SWOT agrees well with existing DOV products in both components. Correlation analyses between DOV datasets and seafloor topographic slopes in typical regions with different seafloor topographic characteristics indicate that SDUST2025DOV_SWOT and SWOT_04DOV exhibit stronger consistency with short-wavelength seafloor topographic signals than SIO V33.1DOV. Independent shipborne gravity observations

https://doi.org/10.5194/essd-2026-712
Preprint. Discussion started: 21 September 2026

show that the RMS difference between SDUST2025GRA_SWOT and shipborne gravity anomalies is 3.82 mGal at the global scale, which is reduced by 0.71, 0.22, and 0.31 mGal compared with SIO V33.1GRA, DTU21GRA, and SWOT_04GRA, respectively. Regional assessments further demonstrate that the dataset achieves more pronounced improvements in areas with complex seafloor topography. In a region containing both seamounts and trenches, the RMS difference of SDUST2025GRA_SWOT is reduced by up to 0.90 mGal compared with SIO V33.1GRA. The SDUST2025DOV_SWOT and SDUST2025GRA_SWOT are available at https://doi.org/10.5281/zenodo.21408557 (Zhang et al., 2026).

1 Introduction

Marine deflection of the vertical (DOV) and gravity anomalies are important parameters for marine gravity field modeling. They provide essential data and theoretical support for navigation and positioning, seafloor topography inversion, resource exploration, and marine engineering construction (Sandwell et al., 2014; Salajegheh et al., 2025; de Vargas et al., 2026; Han et al., 2026; Zhu et al., 2026). Therefore, constructing global marine DOV and gravity anomaly models with high accuracy and high spatial resolution is of great significance for improving marine gravity field models, enhancing marine spatial information services, and supporting marine scientific research and engineering applications.

The successful launch of satellite altimetry missions, together with the continuous deployment of subsequent altimetry satellites, has provided essential observational data for constructing global marine DOV and gravity anomaly models (Liang et al., 2020; Ling et al., 2021; Wan et al., 2022). Conventional radar altimetry satellites mainly adopt a nadir-looking along-track observation mode and can provide high precision one-dimensional (1D) sea surface height (SSH) measurements along satellite ground tracks. These observations have played an important role in the construction of global marine geoid, DOV, and gravity anomaly models (Zhang et al., 2017; Zhu et al., 2020; Anderson et al., 2021; Jin et al., 2022;). However, owing to the limitations of orbital spacing and observation mode, conventional nadir altimetry data provide relatively limited information in the cross-track direction. This limitation may lead to an imbalance in the accuracy of the meridian and prime vertical components of the derived DOV, thereby further affecting the accuracy of subsequent gravity anomaly recovery (Wan et al., 2020; Ji et al., 2021; Jin et al., 2022). Although laser altimetry satellites

https://doi.org/10.5194/essd-2026-712
Preprint. Discussion started: 21 September 2026

developed subsequently can acquire SSH information along multiple tracks through multi-beam observations, cross-track spacing still exists between different beams. Moreover, the observations from different beams are not strictly simultaneous, and the resulting measurements may therefore contain oceanic time-varying signals (Che et al., 2021; Yu et al., 2021; Chao et al., 2023; Peng et al., 2024). In recent years, the successful launch of the Surface Water and Ocean Topography (SWOT) mission has provided a new technical approach for ocean observation (Hwang and Yu, 2024). Unlike conventional nadir-looking altimetry satellites, SWOT is capable of acquiring two-dimensional (2D) SSH observations over a wide swath. These data can directly characterize the 2D spatial structure of the sea surface and provide additional spatial information in the cross-track and other directions. Therefore, SWOT provides a new spatial data basis for deriving high accuracy and high resolution marine DOV and gravity anomaly models (Guo et al., 2024; Wang et al., 2024; Li et al., 2025; Sun et al., 2025).

In the construction of marine DOV products, the remove-compute-restore (RCR) technique is commonly applied to process SSH data derived from satellite altimetry. In this approach, ocean dynamic signals and long-wavelength gravity field signals are first separated from the SSH observations. The residual geoid heights or their gradient information are then used to derive marine DOVs, which can be further applied to recover marine gravity anomalies (Hwang et al., 1998). However, when DOV products are constructed using the RCR technique, their long-wavelength components generally depend on the long-wavelength characteristics of the adopted reference gravity field model. Consequently, the resulting DOV products are constrained, to some extent, by the accuracy of the reference field. In addition, due to the effects of ocean dynamic variability, altimetry noise, and data processing errors, it remains difficult to directly extract residual geoid heights with high accuracy (Chen et al., 2025; Wu et al., 2025). For conventional 1D along-track altimetry satellites, DOVs are usually derived from along-track residual geoid height gradients (Zhu et al., 2022; Zhang et al., 2025). For altimetry satellites equipped with three pairs of laser beams, the multi-beam observation geometry can be used to compute residual geoid height gradients in both the along-track and cross-track directions, which are then used to estimate DOVs (Li et al., 2024). The SWOT/KaRIn wide-swath altimetry mission can provide 2D gridded SSH observations. This allows residual geoid height gradients to be extended beyond the along-track direction to the cross-track, oblique, and diagonal directions. Several

https://doi.org/10.5194/essd-2026-712
Preprint. Discussion started: 21 September 2026

approaches have been developed to derive DOVs from SWOT observations based on directional gradients of residual geoid heights (Yu and Hwang, 2025; Zhu et al., 2025; Guo et al., 2026; Li et al., 2026; Xiao et al., 2026). Although several DOV products have been derived from SWOT observations using these approaches, the construction of a global DOV dataset that directly exploits the local 2D SSH structure without relying on the conventional RCR strategy remains an important issue.

To address the need for a high accuracy and high resolution marine DOV dataset derived from SWOT observations, this study presents SDUST2025DOV_SWOT, a global 1′ × 1′ marine DOV dataset generated from SWOT/KaRIn wide-swath altimetry using a local geoid fitting approach. The local geoid fitting approach exploits the 2D spatial structure of SSH observations and avoids the direct dependence of DOV derivation on the conventional RCR strategy. Based on SDUST2025DOV_SWOT, the corresponding global marine gravity anomaly dataset SDUST2025GRA_SWOT is further generated. Section 2 introduces the datasets used in this study. Section 3 describes the generation procedure of the SDUST2025DOV_SWOT and SDUST2025GRA_SWOT datasets, including DOV derivation and gravity anomaly recovery. Section 4 evaluates the quality of the SDUST2025DOV_SWOT and SDUST2025GRA_SWOT datasets using existing global products and independent shipborne gravity anomaly observations. Section 5 provides information on the data availability of the released datasets. Finally, the conclusions are presented in Section 6.

2 Study data

2.1 SWOT/KaRIn wide-swath altimetry data

In the low-rate measurement mode, SWOT/KaRIn provides 2D SSH data with a gridded resolution of 2 km. The products include both Level-2 and Level-3 versions. The L3 product is generated from the L2 product through additional processing, including crossover calibration, noise reduction, and updates to error correction models. It is released in NetCDF format (AVISO/DUACS, 2024). In this study, the SWOT/KaRIn wide-swath altimetry L3 v2.0.1 data released by AVISO are used, covering the period from cycle 002 to cycle 034. Specifically, the variable "ssha_filtered" is selected as the sea surface height anomaly data. This variable has been corrected for multiple error sources, including instrumental errors, dry and wet tropospheric delays, ionospheric delay, solid Earth tides, ocean tides, load tides, internal tides, pole tides, and dynamic atmospheric correction. In addition, the variable "mss"

https://doi.org/10.5194/essd-2026-712
Preprint. Discussion started: 21 September 2026

is used as the mean sea surface data. This variable is derived from a hybrid mean sea surface model that combines the SIO 22, CNES_CLS22, and DTU21 mean sea surface models (Laloue et al., 2025).

In addition, Absolute Dynamic Topography (ADT) data are used in this study. The ADT product is processed by SSALTO/DUACS and distributed by AVISO. It is an L4 gridded product generated by merging sea surface height data from SARAL/AltiKa, CryoSat-2, HaiYang-2B, Jason-3, Sentinel-3A/B, Sentinel-6A, SWOT nadir, and SWOT/KaRIn L3 observations (SSALTO/DUACS, 2025).

2.2 Global marine DOV and gravity anomaly products

To evaluate the global marine DOV and gravity anomaly datasets constructed in this study, three global marine gravity field products, namely DTU21 (Andersen et al., 2023), SIO V33.1 (Sandwell et al., 2021), and SWOT_04 (Yu et al., 2024), are selected for comparison. Among them, DTU21 and SIO V33.1 are marine gravity anomaly products constructed mainly from conventional 1D along-track altimetry data. In contrast, SWOT_04 is a marine gravity anomaly product developed by incorporating SWOT/KaRIn wide-swath altimetry data into the V33.1 framework. In addition, SIO V33.1 and SWOT_04 also provide global marine DOV products.

A reference gravity field model needs to be removed when deriving the global marine gravity anomaly dataset. In this study, the XGM2019e_2159 model, expanded to degree and order 2190, is selected as the reference gravity field model. This model is publicly available from the ICGEM website (Zingerle et al., 2020). The corresponding reference DOV and gravity anomaly models can be obtained based on this reference gravity field model.

2.3 Shipborne gravity anomaly data

To further evaluate the accuracy of the global marine gravity anomaly dataset constructed in this study, global shipborne gravity anomaly data provided by the U.S. National Centers for Environmental Information (NCEI) and the Japan Agency for Marine-Earth Science and Technology (JAMSTEC) are used as independent external validation data. Shipborne gravity anomaly data are in situ observations and can provide marine gravity information with relatively high accuracy and high spatial resolution along ship tracks. Considering that early shipborne gravity data were strongly affected by factors such as navigation and positioning accuracy, only shipborne gravity anomaly data collected after 1990 are used for model accuracy validation in this study.

https://doi.org/10.5194/essd-2026-712
Preprint. Discussion started: 21 September 2026

Specifically, 490 ship tracks from NCEI and 728 ship tracks from JAMSTEC are selected, as shown in Fig. 1.

During shipborne gravity surveys, some observations may contain gross errors due to factors such as instrument status, measurement environment, navigation conditions, and data recording. To improve the quality of the shipborne gravity anomaly data, gross errors are first removed using the three-sigma criterion, with the XGM2019e_2159 reference gravity anomaly model used as the benchmark. On this basis, the differences between the shipborne gravity anomalies and the reference model along each ship track are further fitted using a linear model. This step is used to correct the constant bias and linear drift errors in the shipborne gravity anomaly data (Hwang and Parsons, 1995).

After the above processing, 11,716,306 valid shipborne gravity anomaly measurements are retained from the NCEI dataset, with a data rejection rate of 1.35%. For the JAMSTEC dataset, 36,316,208 valid shipborne gravity anomaly measurements are retained, with a data rejection rate of 1.30%. Considering the large amount of redundant information in the shipborne gravity data, a 0.5 km median filtering procedure is applied along the ship tracks. Finally, a total of 10,194,443 shipborne gravity anomaly measurements are obtained. Table 1 presents the statistical differences between the shipborne gravity anomaly data and the XGM2019e_2159 reference gravity anomaly model before and after data processing. As shown in the table, the STD of the differences between the original shipborne gravity anomaly data and the XGM2019e_2159 reference model is 8.95 mGal. After gross error removal, ship-track correction, and median filtering, the STD and RMS of the differences both decrease to 4.66 mGal. This indicates that the quality of the shipborne gravity anomaly data is significantly improved after processing. Therefore, the processed shipborne gravity data have good reliability and can be used as independent validation data for the subsequent accuracy assessment of gravity anomaly datasets.

Table 1. Statistics of the differences between shipborne gravity anomalies and the XGM2019e_2159 reference gravity anomaly model (Unit: mGal)

Data Status	Model	MAX	MIN	MEAN	STD	RMS
Before Processing	XGM2019e_2159	933.10	-1001.81	1.45	8.95	9.07
After Processing	XGM2019e_2159	86.86	-99.48	-0.01	4.66	4.66

https://doi.org/10.5194/essd-2026-712
Preprint. Discussion started: 21 September 2026

Open Access Earth System Science Data Discussions

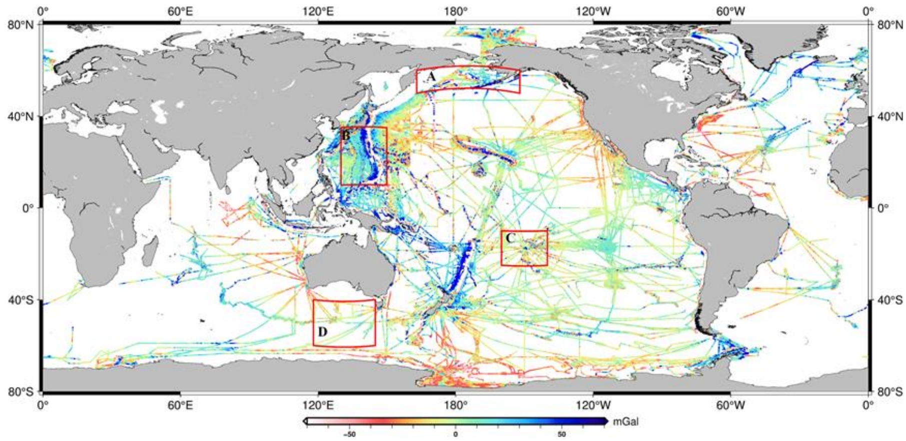

Figure 1. Spatial Distribution of Processed NCEI and JAMSTEC Shipborne Gravity Anomaly Data Since 1990

3 Methodology

3.1 Generation of marine DOV dataset

3.1.1 DOV estimation at SWOT/KaRIn observation points

SWOT/KaRIn wide-swath measurement mode provides 2D gridded SSH observations. By removing the ADT from the SSH data, the corresponding 2D gridded geoid heights can be obtained, which are expressed as

$$N = SSHA + MSS - ADT \tag{1}$$

where N denotes the geoid height, $SSHA$ represents the sea surface height anomaly, MSS denotes the hybrid mean sea surface model, and ADT represents the absolute dynamic topography. A local 3′×3′ computational window is established with a given observation point within the swath as its center. The geoid height data at all observation points within the window are then used for spatial plane fitting to approximate the local geoid over the window. The geoid is an equipotential surface of the Earth's gravity field, and its normal direction therefore provides an approximation of the local vertical direction, namely, the direction of gravity. Meanwhile, the ellipsoidal normal at the center of the window can be determined from the parameters of the reference ellipsoid. The angular deviation between the local geoid normal and the reference ellipsoid normal represents the DOV at the center point. By resolving this angular deviation in the meridian and prime vertical directions, the meridian and prime vertical components of the DOV are obtained, respectively.

When fitting the local geoid within the computational window, principal component analysis (PCA) is employed in this study. First, the coordinates of the observation points P within the window are transformed from the geodetic coordinate system to the Earth-centered, Earth-fixed (ECEF) Cartesian coordinate system. The geometric centroid of all observation points in the window is then calculated, and the point coordinates are centered by subtracting this centroid. Based on the centered coordinates, the covariance matrix is constructed as follows

$$\bar{P} = \frac{1}{m}\sum_{i=1}^{m} P_i \tag{2}$$

$$\mathbf{C} = \frac{1}{m-1}\sum_{i=1}^{m}(P_i - \bar{P})(P_i - \bar{P})^T \tag{3}$$

where $\bar{P}$ denotes the coordinates of the geometric centroid of the observation points within the window, **C** is the covariance matrix, m is the number of observation points within the local window. After eigenvalue decomposition is performed on the covariance matrix **C**, three eigenvalues and their corresponding eigenvectors are obtained. The eigenvalues are sorted in descending order as $\lambda_1 \geq \lambda_2 \geq \lambda_3$, with the corresponding eigenvectors denoted by $\boldsymbol{v}_1$, $\boldsymbol{v}_2$, and $\boldsymbol{v}_3$, respectively. Since the observation points within the local window have the smallest dispersion in the direction normal to the fitted plane, the eigenvector $\boldsymbol{v}_3$ corresponding to the smallest eigenvalue λ_3 is taken as the normal vector of the locally fitted geoid plane and is used to approximate the local gravity direction, denoted as $\boldsymbol{g}_p = \boldsymbol{v}_3$. The locally fitted geoid plane can then be expressed as

$$\boldsymbol{g}_p^T(P - \bar{P}) = 0 \tag{4}$$

The reference ellipsoid normal direction vector at the center point of the local window is determined from the reference ellipsoid parameters and then normalized to obtain the unit vector $\boldsymbol{u}$. Based on this normal vector and the ECEF coordinates of the center point, a local East-North-Up (ENU) Cartesian coordinate system is established at the window center. The east, north, and up components of the locally fitted plane normal vector can then be expressed as follows

$$\begin{cases} d_e = \boldsymbol{g_p} \cdot \boldsymbol{e} \\ d_n = \boldsymbol{g_p} \cdot \boldsymbol{n} \\ d_u = \boldsymbol{g_p} \cdot \boldsymbol{u} \end{cases} \tag{5}$$

where $\boldsymbol{e}$ and $\boldsymbol{n}$ denote the east and north unit vectors of the local ENU coordinate system, respectively, and d_e, d_n, d_u are the east, north, and up components of the gravity direction vector $\boldsymbol{g}_p$ respectively. The meridian component of the DOV is defined as the inclination of the local gravity direction vector relative to the reference ellipsoid normal in the north-up plane, whereas the prime vertical component is defined as the corresponding inclination in the east-up plane. Therefore, the meridian component and the prime vertical component of the DOV can be expressed as follows

$$\begin{cases} \xi = \arctan(d_n / d_u) \\ \eta = \arctan(d_e / d_u) \end{cases} \tag{6}$$

where ξ is the meridian component, η represent the prime vertical component.

3.1.2 Gridded DOV

SWOT/KaRIn observation points have a spatial resolution of approximately 2 km, and their data organization differs from that of commonly used marine gravity field products on a regular 1′ grid. To obtain a global marine DOV dataset in a regular gridded format, the region spanning longitudes 0°-360° and latitudes -77.6°-77.6° is first discretized into a regular grid at 1′ intervals. Land areas are then masked using the GEBCO2025 bathymetric dataset, and only ocean grid points are retained. Subsequently, a 2′ search window is established around each ocean grid point to identify SWOT/KaRIn DOV observations within the window. The DOV values at these observations are interpolated to the corresponding grid point using inverse-distance-squared weighting. After the calculation for the current grid point is completed, the search window is sequentially moved to the next ocean grid point, and the same search and interpolation procedure is repeated. This process continues until the meridian and prime vertical components of the DOV are gridded for all ocean grid points across the

https://doi.org/10.5194/essd-2026-712
Preprint. Discussion started: 21 September 2026

global ocean.

3.2 Derivation of gravity anomalies

Based on the gridded DOV data, gravity anomalies can be derived using the inverse Vening Meinesz formula, which is expressed as follows (Hwang, 1998)

$$\Delta g(P) = \frac{\gamma_0}{4\pi}\iint H'(\psi)(\xi_Q \cos\alpha_{QP} + \eta_P \sin\alpha_{QP})d\sigma_Q \tag{7}$$

where γ_0 denotes the normal gravity at point P, α_{QP} is the azimuth from point Q to point P, $H'(\psi)$ denotes the kernel function, which can be expressed as follows

$$H'(\psi) = -\frac{\cos\frac{\psi}{2}}{2\sin^2\frac{\psi}{2}} + \frac{\cos\frac{\psi}{2}(2\sin\frac{\psi}{2}+3)}{2\sin\frac{\psi}{2}(\sin\frac{\psi}{2}+1)} \tag{8}$$

It can be seen from the kernel function that a singularity occurs when $\psi = 0$. Therefore, when points P and Q are sufficiently close to each other, the surrounding region is defined as the inner zone. This region is generally approximated as a circular area, and the gravity anomaly contribution within it is evaluated separately.

4 Characteristics and quality assessment of the datasets

4.1 Description of the global marine DOV and gravity anomaly datasets

4.1.1 Global marine DOV dataset

SWOT/KaRIn operates in a wide-swath measurement mode, with an approximately 20 km observation gap near the nadir track. In addition, gaps may occur between adjacent passes at low latitudes. To improve the spatial continuity of the data, the Kriging interpolation method proposed by Ya et al. (2026) is first applied to fill the nadir gap and the inter-pass gaps in low latitude regions. Based on the gap-filled sea surface height data from 33 cycles, geoid heights at individual observation points are first derived from the SSH and ADT data using Eq. (1). To reduce the influence of gross errors on subsequent DOV determination, a three-sigma criterion is applied to the geoid height observations from all 33 cycles for outlier rejection. Subsequently, for each cycle, a $3'\times3'$ local window is used as the computational unit. Principal component analysis (PCA) is employed to fit the local geoid within each window. The WGS84 ellipsoid is adopted as the reference ellipsoid, and the meridian and prime vertical components of the DOV at individual observation points are then derived following the method described in Section 3.1.1. To further reduce the influence of random errors, DOV estimates at the same locations along corresponding tracks from different cycles are

https://doi.org/10.5194/essd-2026-712
Preprint. Discussion started: 21 September 2026

averaged, yielding the multi-cycle-averaged meridian and prime vertical DOV components at the observation points.

Although the orbital inclination of SWOT/KaRIn is approximately 77.6°, valid sea surface height observations can extend beyond 77.6°N and 77.6°S owing to the mission's wide-swath observation geometry. In the subsequent construction of the gridded DOV dataset, observation points within a 2′ neighborhood of each grid point are required. In addition, a 1° integration radius is adopted for gravity anomaly recovery. To ensure the completeness of the calculations in the boundary regions, the latitude range of the SSH data used for DOV determination is therefore extended to 80°N and 80°S. Owing to limitations in computational resources, the global domain is divided into two regions, both spanning 0°-360° in longitude: one extending from -80° to 1° and the other from -1° to 80°. The DOV components in the two regions are gridded separately following the method described in Section 3.1.2, and the results within the overlapping region near the equator are merged by averaging.

After the preliminary global marine DOV grids are obtained, a small number of unfilled gaps and localized anomalous values remain in high latitude sea-ice regions and some nearshore areas. According to the SWOT/KaRIn data documentation, observations in high latitude, nearshore, and sea-ice-covered regions may still be affected by tilt errors and other residual errors (AVISO/DUACS, 2024). To improve the overall spatial continuity and stability of the dataset, two additional procedures are applied in this study. For unfilled ocean grid points located more than 3 km offshore, Kriging interpolation is performed using the eight surrounding valid values. In addition, the global marine DOV dataset derived in this study is compared with the DOV values computed from the XGM2019e_2159 reference gravity field model. For anomalous grid points where the absolute difference exceeds 100 μrad, the corresponding DOV values from XGM2019e_2159 are used as replacements. The replacement rates are only 0.0004% and 0.0005% for the meridian and prime vertical components, respectively, indicating that such anomalous grid points are extremely rare and have a negligible effect on the overall dataset.

After the above processing, SDUST2025DOV_SWOT, a complete global marine DOV dataset with a grid resolution of 1′ ×1′, is obtained over the region spanning longitudes from 0° to 360° and latitudes from -77.6° to 77.6°, as shown in Fig. 2. The dataset is available at https://doi.org/10.5281/zenodo.21408557 (Zhang et al., 2026). Hereafter, the dataset is referred to as SDUST2025DOV. To distinguish the sources of

https://doi.org/10.5194/essd-2026-712
Preprint. Discussion started: 21 September 2026

Open Access Earth System Science Data Discussions

the DOV values at different grid points, a flag variable is included in the NetCDF file. This variable contains four categories. A value of flag = 0 indicates that the DOV value at the grid point is obtained by gridding the PCA plane fitting results using inverse-distance-squared weighting. A value of flag = 1 indicates an unfilled ocean grid point located more than 3 km offshore, for which the DOV value is obtained by Kriging interpolation using the eight surrounding valid neighboring values. A value of flag = 2 indicates that the absolute difference between the DOV derived in this study and that from XGM2019e_2159 exceeds 100 μrad; the corresponding DOV value is therefore replaced by the XGM2019e_2159 value. Finally, flag = 3 indicates that the grid point is located over land or in a nearshore region without valid SSH observations. In such cases, the DOV cannot be derived from SWOT/KaRIn data, and the corresponding value from XGM2019e_2159 is used directly to fill the grid point.

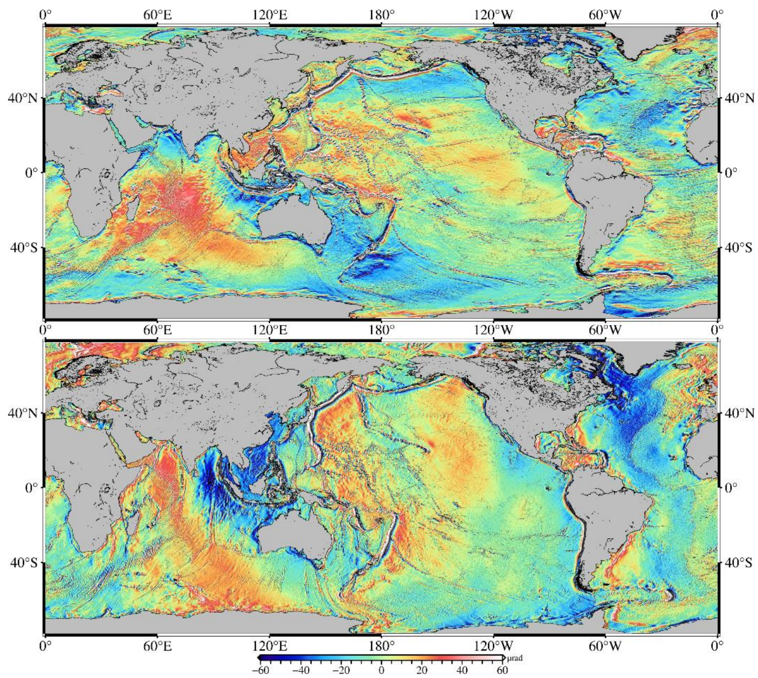

Figure 2. SDUST2025DOV dataset. The upper panel shows the meridian component, and the lower panel shows the prime vertical component.

4.1.2 Global marine gravity anomaly dataset

The global marine gravity anomaly dataset is derived from the SDUST2025DOV dataset. First, the XGM2019e_2159 reference DOV model is removed to obtain the residual DOV field. Residual marine gravity anomalies are then derived within a

https://doi.org/10.5194/essd-2026-712
Preprint. Discussion started: 21 September 2026

1°integration radius using a 1D fast Fourier transform technique and the inverse Vening-Meinesz formula described in Section 3.2. Finally, the XGM2019e_2159 reference gravity anomaly field is restored to obtain the complete marine gravity anomaly dataset. Owing to limitations in computational resources, the global ocean domain is divided into 144 computational blocks, each covering 20°×20°. To reduce boundary effects between adjacent blocks, each block is extended outward by 1° during the computation. After the calculations are completed, the extended margins are removed, and the individual block results are mosaicked. The resulting global 1′×1′ marine gravity anomaly dataset, SDUST2025GRA_SWOT, covers longitudes from 0° to 360° and latitudes from -77.6° to 77.6°, as shown in Fig. 3. The dataset is available at https://doi.org/10.5281/zenodo.21408557 (Zhang et al., 2026). Hereafter, the dataset is referred to as SDUST2025GRA.

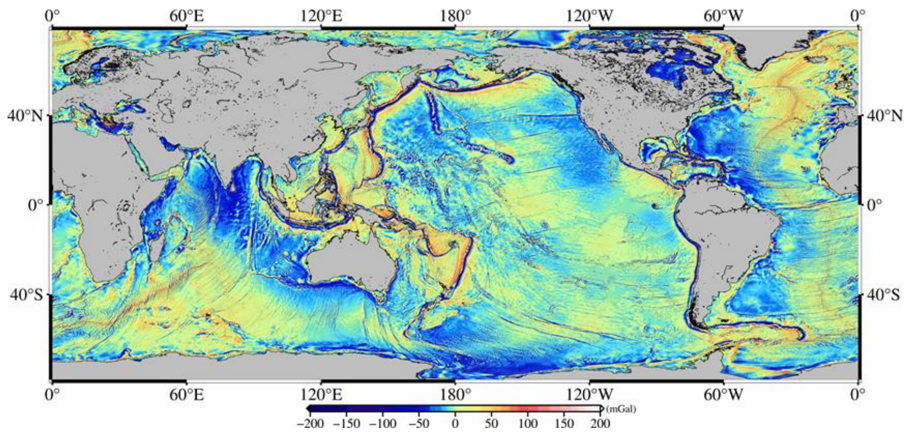

Figure 3. SDUST2025GRA dataset.

4.2 Quality assessment of the marine DOV dataset

4.2.1 Global assessment of DOV datasets

Given the difficulty of obtaining direct in situ marine DOV observations, the quality of the SDUST2025DOV dataset is assessed through comparisons with the widely recognized SIO V33.1DOV and SWOT_04DOV products. In these comparisons, only grid points with flag values of 0, 1, and 2 are used, whereas grid points with flag = 3 are excluded. The comparisons are conducted over the region spanning longitudes from 0° to 360° and latitudes from -77.6° to 77.6°, and the statistical results of the differences are presented in Table 2.

Table 2. Statistics of Differences Between SDUST2025DOV and Two Reference DOV Products: SIO V33.1 DOV and SWOT_04DOV (Unit: μrad)

https://doi.org/10.5194/essd-2026-712
Preprint. Discussion started: 21 September 2026

Component	Product Difference	MAX	MIN	MEAN	STD	RMS
ξ	SDUST2025DOV-SIO V33.1 DOV	134.94	-187.38	0.06	1.41	1.41
	SDUST2025DOV-SWOT_04 DOV	134.94	-187.29	0.00	1.41	1.41
η	SDUST2025DOV-SIO V33.1 DOV	129.24	-165.87	0.02	1.63	1.63
	SDUST2025DOV-SWOT_04 DOV	129.24	-164.90	0.01	1.56	1.56

As shown in Table 2, over the latitude range from -77.6° to 77.6°, the STDs of the meridian component differences between SDUST2025DOV and both SIO V33.1 DOV and SWOT_04DOV are 1.41 μrad, indicating good consistency among the three products in the meridian component. For the prime vertical component, the STD of the differences between SDUST2025DOV and SWOT_04DOV is 1.56 μrad, slightly lower than the corresponding value of 1.63 μrad obtained for SIO V33.1 DOV. A possible explanation is that SWOT_04DOV is constructed by incorporating SWOT/KaRIn altimetry data into the SIO V33.1 DOV framework, whereas SDUST2025DOV is also derived from 2D SWOT/KaRIn wide-swath observations. Consequently, the two products exhibit relatively higher consistency in the prime vertical component. In contrast, the meridian component is generally better constrained by conventional along-track altimetry observations, which may partly explain the relatively small differences among the three products. Therefore, no substantial reduction in the STD of the meridian component differences is observed after incorporating SWOT observations. Overall, SDUST2025DOV shows good agreement with both reference products in the meridian and prime vertical components, demonstrating the good quality of the SDUST2025DOV dataset.

4.2.2 Regional assessment of DOV products under different seafloor topographic conditions

To further investigate the performance of different DOV products under different seafloor topographic conditions, four representative regions, denoted A, B, C, and D in Fig. 1, are selected for analysis. Region A is located near the Aleutian Islands. Its seafloor morphology is mainly controlled by the Aleutian Trench and the adjacent trench-arc transition zone. The Bering Sea lies to the north. Seamounts are relatively sparse within this region, whereas pronounced water-depth variations occur near the trench (Witter et al., 2022). Region B is located in the eastern Philippine Sea. It contains the Mariana Trench and multiple seamounts. The region is characterized by strong seafloor relief and complex gravity field variations (Sdrolias and Müller, 2006). Region C is situated near the Society Islands and is strongly influenced by hotspot volcanism. Numerous volcanic islands and seamounts occur within this region. It is characterized

https://doi.org/10.5194/essd-2026-712
Preprint. Discussion started: 21 September 2026

by a well-developed hotspot seamount chain (Allain et al., 2008). Region D is located south of Australia. The seafloor topography is relatively smooth, with no pronounced concentrations of seamounts or strong tectonic relief. For each of the four regions, differences between SDUST2025DOV and SIO V33.1 DOV are statistically evaluated. The same statistical assessment is also performed between SDUST2025DOV and SWOT_04DOV. The resulting statistics are presented in Table 3, while the spatial distributions of the differences between DOV products are shown in Figs. 4-7.

Table 3. Regional Statistics of Differences Between SDUST2025DOV and Two Reference DOV Products: SIO V33.1 DOV and SWOT_04DOV (Unit: μrad)

Component	Region	SDUST2025DOV vs SIO V33.1 DOV		SDUST2025DOV vs SWOT_04 DOV	
		MEAN	RMS	MEAN	RMS
ξ	A	0.12	1.94	-0.03	1.83
	B	0.08	1.28	0.03	1.33
	C	-0.02	1.36	-0.01	1.34
	D	-0.17	0.60	-0.05	0.77
η	A	0.03	1.70	0.01	1.59
	B	-0.03	1.61	-0.18	1.48
	C	-0.09	1.55	-0.08	1.39
	D	0.00	0.80	-0.11	0.91

Table 3 shows a consistent pattern in Regions B, C, and D. For both comparisons with SIO V33.1 DOV and SWOT_04DOV, the RMS of the meridian component differences is lower than those of the prime vertical component differences. Region A shows the opposite pattern. In this region, the RMS of the meridian component differences is higher than those of the prime vertical component differences. The spatial distribution shown in Fig. 4 helps explain this contrast. Region A is mainly influenced by the Aleutian Trench and the adjacent island-arc topography. These geomorphic features extend approximately in an east-west direction. Consequently, the associated topographic variations and gravity field signals are more pronounced in the north-south direction. This directional characteristic may explain the larger differences among the DOV products in the meridian component near the trench and island arc.

In Region B, the STD of the meridian component differences between SDUST2025DOV and V33.1 DOV is lower than that between SDUST2025DOV and SWOT_04DOV. Fig. 5 shows relatively pronounced differences between SDUST2025DOV and SWOT_04DOV in the ocean area off southeastern Japan. This region is strongly affected by ocean dynamic processes such as the Kuroshio Extension and mesoscale eddies. The associated temporal variability of sea surface height may influence the derived DOV estimates. Although both SDUST2025DOV and SWOT_04DOV incorporate SWOT/KaRIn altimetry data, they use different data

https://doi.org/10.5194/essd-2026-712
Preprint. Discussion started: 21 September 2026

versions and processing strategies. SWOT_04DOV is based on SWOT/KaRIn L2 data, whereas this study uses L3 data. The L3 product undergoes additional denoising and post-processing based on the L2 product. Therefore, differences between the two processed datasets may become more pronounced in regions with strong ocean dynamic variability. This may further increase the differences between the resulting DOV products (Dibarboure et al., 2025).

For the prime vertical component in Region B, the STD of the differences between SDUST2025DOV and SWOT_04DOV is lower than that between SDUST2025DOV and V33.1 DOV. This suggests improved consistency in the prime vertical direction between DOV products constructed from SWOT/KaRIn wide-swath altimetry data. The improved consistency may be related to the additional cross-track information provided by the 2D SWOT/KaRIn observations, which is relatively limited in conventional nadir altimetry. This may help reduce the imbalance in accuracy between the meridian and prime vertical DOV components. This feature is more evident in Region C, which is dominated by seamount structures. The STDs of the meridian and prime vertical component differences between SDUST2025DOV and SWOT_04DOV are relatively similar. This indicates good consistency between the two SWOT/KaRIn-based DOV products in regions with pronounced 2D seafloor relief. In Region D, the situation is different. No prominent trenches, seamounts, or other strong topographic features are present, and the gravity field varies relatively smoothly. As a result, the differences between SDUST2025DOV and the two reference DOV products are similar for both the meridian and prime vertical components.

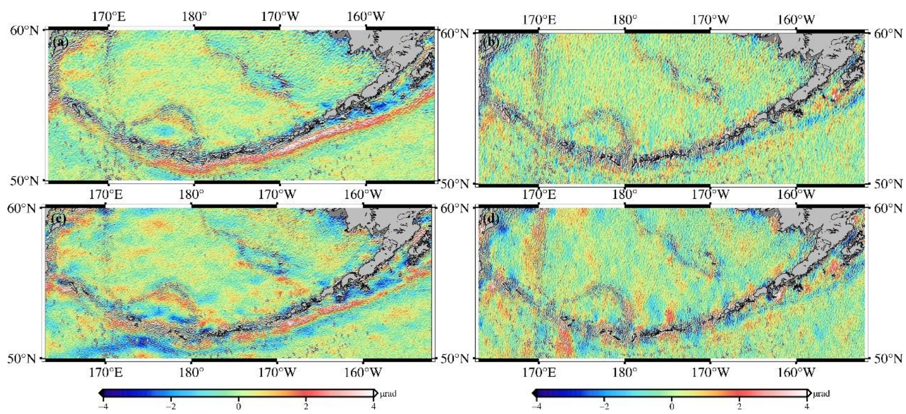

Figure 4. Spatial distributions of DOV differences in Region A. Panels (a) and (b) show the meridian and prime vertical components of the differences between SDUST2025DOV and SIO V33.1 DOV, respectively. Panels (c) and (d) show the corresponding components of the

https://doi.org/10.5194/essd-2026-712
Preprint. Discussion started: 21 September 2026

Open Access Earth System Science Data Discussions

differences between SDUST2025DOV and SWOT_04DOV, respectively.

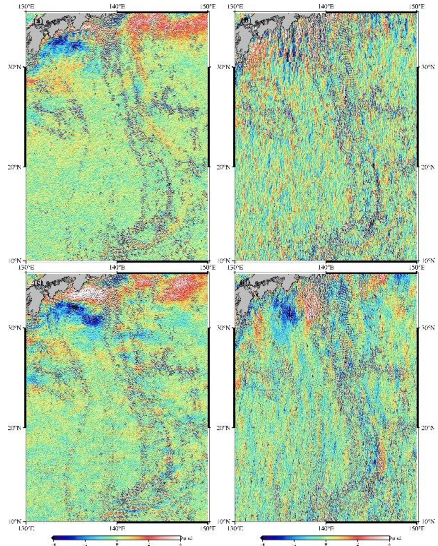

Figure 5. Spatial distributions of DOV differences in Region B. Panels (a) and (b) show the meridian and prime vertical components of the differences between SDUST2025DOV and SIO V33.1 DOV, respectively. Panels (c) and (d) show the corresponding components of the differences between SDUST2025DOV and SWOT_04DOV, respectively.

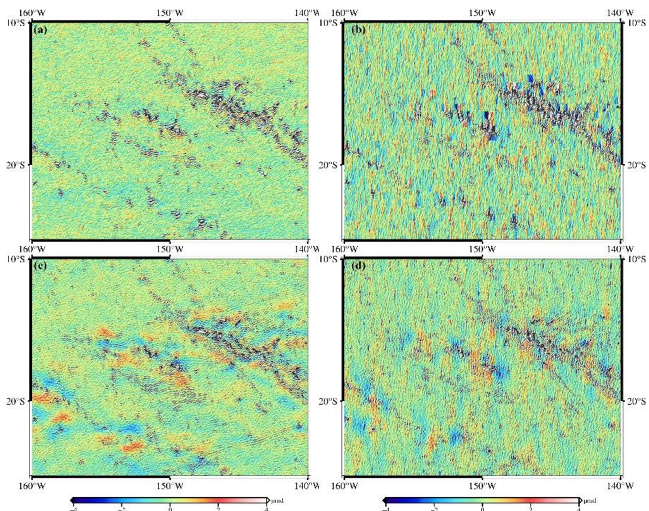

Figure 6. Spatial distributions of DOV differences in Region C. Panels (a) and (b) show the meridian and prime vertical components of the differences between SDUST2025DOV and SIO V33.1 DOV, respectively. Panels (c) and (d) show the corresponding components of the differences between SDUST2025DOV and SWOT_04DOV, respectively.

https://doi.org/10.5194/essd-2026-712
Preprint. Discussion started: 21 September 2026

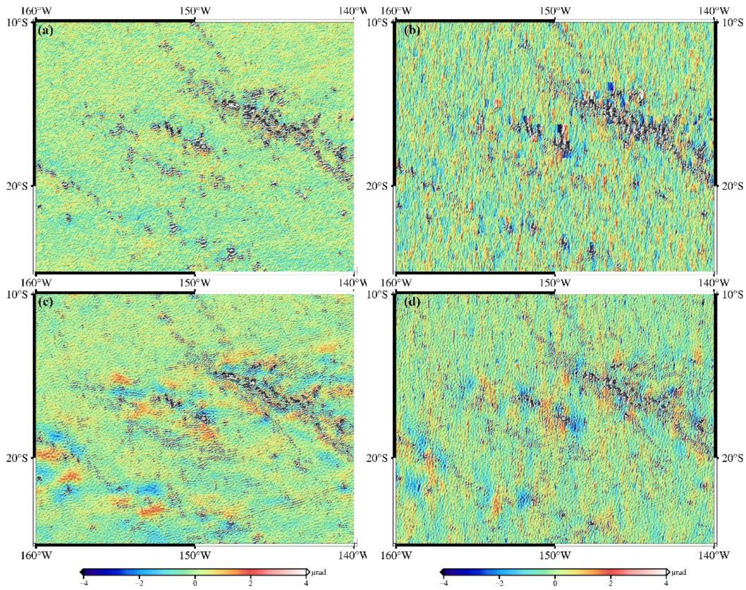

Figure 7. Spatial distributions of DOV differences in Region D. Panels (a) and (b) show the meridian and prime vertical components of the differences between SDUST2025DOV and SIO V33.1 DOV, respectively. Panels (c) and (d) show the corresponding components of the differences between SDUST2025DOV and SWOT_04DOV, respectively.

Inspection of the spatial difference maps for the four regions reveals clear banded patterns in the prime vertical component of the differences between SDUST2025DOV and SIO V33.1 DOV. Similar banded errors are also present, although to a lesser extent, in the differences between SDUST2025DOV and SWOT_04DOV. A possible explanation is related to the observation geometry of the altimetry datasets used to generate these DOV products. SIO V33.1 DOV is derived mainly from conventional 1D along-track altimetry data. Cross-track information is therefore relatively limited, making the prime vertical component more susceptible to directional errors. SWOT_04DOV incorporates SWOT/KaRIn wide-swath altimetry data. However, SWOT/KaRIn observations contain an approximately 20 km nadir gap as well as swath-edge gaps at low latitudes. SWOT_04DOV fills these areas using SIO V33.1 DOV data. As a result, the prime vertical characteristics of SIO V33.1 DOV are partly retained within these gap regions. This may explain why pronounced banded differences appear in the prime vertical component maps for both comparisons. The difference maps also show that some areas of disagreement correspond spatially to seafloor features such as trenches and seamounts. To further investigate whether these topography-related differences are related to the ability of different DOV products to capture seafloor-

https://doi.org/10.5194/essd-2026-712
Preprint. Discussion started: 21 September 2026

Open Access Earth System Science Data Discussions

related signals, a band-pass filtering method is applied. Correlation coefficients between each DOV product and seafloor topographic slope are then calculated for different wavelength bands. The results are presented in Tables 4 and 5.

Table 4. Correlation Coefficients Between the Meridian Components of Three DOV Products and Seafloor Topographic Slope at Different Wavelength Bands

Region	Wavelength Bands (km)	SIO V33.1 DOV	SWOT_04 DOV	SDUST2025DOV
A	[10.0,50.0)	0.5011	0.5219	0.5253
	[50.0,100.0)	0.6652	0.6640	0.6630
	[100.0,1000.0]	0.7077	0.7075	0.7121
B	[10.0,50.0)	0.4929	0.5253	0.5126
	[50.0,100.0)	0.5889	0.5888	0.5893
	[100.0,1000.0]	0.6799	0.6802	0.6805
C	[10.0,50.0)	0.5729	0.6074	0.5866
	[50.0,100.0)	0.7146	0.7136	0.7158
	[100.0,1000.0]	0.7871	0.7884	0.7896
D	[10.0,50.0)	0.4915	0.5366	0.5102
	[50.0,100.0)	0.6053	0.5975	0.6116
	[100.0,1000.0]	0.4500	0.4504	0.4498

Table 5. Correlation Coefficients Between the Prime Vertical Components of Three DOV Products and Seafloor Topographic Slope at Different Wavelength Bands

Region	Wavelength Bands (km)	SIO V33.1 DOV	SWOT_04 DOV	SDUST2025DOV
A	[10.0,50.0)	0.4946	0.5213	0.5216
	[50.0,100.0)	0.6265	0.6269	0.6248
	[100.0,1000.0]	0.5819	0.5813	0.5846
B	[10.0,50.0)	0.4986	0.5368	0.5192
	[50.0,100.0)	0.6540	0.6537	0.6536
	[100.0,1000.0]	0.6915	0.6930	0.6933
C	[10.0,50.0)	0.5490	0.5858	0.5665
	[50.0,100.0)	0.6449	0.6434	0.6442
	[100.0,1000.0]	0.7328	0.7341	0.7344
D	[10.0,50.0)	0.5364	0.5748	0.5556
	[50.0,100.0)	0.7181	0.7195	0.7214
	[100.0,1000.0]	0.6653	0.6646	0.6644

Tables 4 and 5 show that, in the short-wavelength range of 10-50 km, both SDUST2025DOV and SWOT_04DOV exhibit higher correlations with seafloor topographic slope than SIO V33.1 DOV. This indicates that DOV products based on SWOT/KaRIn altimetry data can better capture local gravity field variations associated with seafloor relief at short wavelengths. A likely reason is that SWOT/KaRIn wide-swath altimetry provides richer 2D spatial information than conventional nadir altimetry. Such observations are more favorable for recovering medium and short wavelength gravity signals in regions characterized by seamounts, trenches, and other pronounced seafloor features. Within the 10-50 km wavelength range, however, the correlation between SDUST2025DOV and seafloor topographic slope is lower than that of SWOT_04DOV. This difference may be related to the different data versions and

https://doi.org/10.5194/essd-2026-712
Preprint. Discussion started: 21 September 2026

processing strategies adopted by the two products. SWOT04_DOV is constructed from 42 cycles of SWOT/KaRIn L2 altimetry data, whereas the SDUST2025DOV is constructed from 33 cycles of SWOT/KaRIn L3 altimetry data. Therefore, SWOT04_DOV uses more altimetry observations than the SDUST2025DOV, which may allow it to retain more short-wavelength topography-related details. In addition, the L3 data used in this study undergo further denoising and post-processing based on the L2 product (Dibarboure et al., 2025). Consequently, SDUST2025DOV shows a slightly weaker short-wavelength correlation with seafloor topographic slope than SWOT_04DOV, while still showing higher correlations than SIO V33.1DOV, which does not incorporate SWOT data.

4.3 Quality assessment of the marine gravity anomaly dataset

4.3.1 Global validation using shipborne gravity observations

Shipborne gravity anomaly data are derived from in situ measurements and therefore provide a relatively independent source for evaluating the accuracy of marine gravity anomaly products. In this study, the processed shipborne gravity anomaly data are used as independent validation data. Differences are calculated separately against SDUST2025GRA, SWOT_04GRA, DTU21 GRA, and SIO V33.1 GRA. The resulting differences are then statistically evaluated, and the results are presented in Table 6.

Table 6. Statistics of Differences Between Shipborne Gravity Anomalies and Gravity Anomaly Products (Unit: mGal)

Region	Product	MAX	MIN	MEAN	STD	RMS
Global [-77.6°, 77.6°]	SIO V33.1 GRA	86.60	-105.33	0.08	4.52	4.53
	DTU21GRA	87.53	-101.03	0.00	4.04	4.04
	SWOT_04GRA	87.30	-100.48	0.16	4.12	4.13
	SDUST2025GRA	86.72	-108.02	0.00	3.82	3.82
Middle and Low Latitudes [-60°, 60°]	SIO V33.1 GRA	86.60	-99.90	0.13	4.28	4.29
	DTU21GRA	87.53	-101.03	0.01	3.89	3.89
	SWOT_04GRA	87.30	-100.48	0.18	3.87	3.87
	SDUST2025GRA	86.72	-100.31	0.02	3.69	3.69
High Latitudes [-77.6°, -60°); (60°, 77.6°]	SIO V33.1 GRA	78.71	-105.33	-0.45	6.44	6.46
	DTU21GRA	68.03	-84.11	-0.17	5.28	5.28
	SWOT_04GRA	80.28	-97.00	-0.06	6.12	6.12
	SDUST2025GRA	72.20	-108.02	-0.14	4.98	4.98

As shown in Table 6, the STD and RMS of the differences between SDUST2025GRA and the shipborne gravity anomaly data are lower than those obtained for SWOT_04GRA, DTU21GRA, and SIO V33.1 GRA. This pattern is consistent across the global ocean, middle and low latitude regions, and high latitude regions. It indicates that SDUST2025GRA shows higher consistency with independent shipborne gravity observations than the other gravity anomaly products.

In middle and low latitude ocean regions, SWOT_04GRA and DTU21GRA show comparable validation accuracy. Both products outperform SIO V33.1GRA. SWOT_04GRA incorporates SWOT/KaRIn wide-swath altimetry data, which partly compensates for the limited cross-track information provided by conventional nadir altimetry. This is beneficial for recovering medium and short wavelength signals of the marine gravity field. In particular, SWOT/KaRIn 2D observations provide relatively good spatial coverage at middle and low latitudes. Gravity anomaly products constructed using SWOT data therefore achieve relatively high accuracy in these regions. DTU21GRA does not incorporate SWOT data. However, it introduces medium and long wavelength corrections based on altimetry and GOCE data, thereby improving upon the conventional remove-restore approach based on EGM2008. As a result, DTU21GRA also achieves good validation accuracy in middle and low latitude ocean regions. At high latitudes, DTU21GRA outperforms SWOT_04GRA and SIO V33.1GRA. This advantage is closely related to its data-processing strategy. In high latitude regions, DTU21GRA applies improved retracking methods to SARAL/AltiKa and CryoSat-2 observations. It also incorporates medium and long wavelength corrections based on altimetry and GOCE data to reduce deficiencies of conventional reference fields at high latitudes (Anderson et al., 2023). These processing strategies contribute to the strong stability and accuracy of DTU21GRA in high latitude ocean regions. In contrast, although the SDUST2025GRA employs the remove-restore technique during gravity anomaly recovery, its underlying DOV product, SDUST2025DOV, is not derived using the conventional remove-restore approach. Instead, it is directly determined by fitting the local geoid surface to the 2D SSH field observed by SWOT/KaRIn. This strategy makes fuller use of the 2D spatial information contained in SWOT/KaRIn observations and reduces the dependence of DOV estimation on the long-wavelength characteristics of the reference gravity field. Consequently, SDUST2025GRA still achieves better validation accuracy against shipborne gravity data even in high latitude ocean regions, where DTU21GRA has a clear advantage. This further confirms the high quality of the SDUST2025GRA dataset for global marine gravity anomaly applications.

https://doi.org/10.5194/essd-2026-712
Preprint. Discussion started: 21 September 2026

4.3.2 Regional validation under different seafloor topographic conditions

For the four regions described above, differences between each gravity anomaly product and the shipborne gravity anomaly data are calculated separately. The corresponding statistics are presented in Table 7.

Table 7. Statistics of Differences Between Shipborne Gravity Anomalies and Gravity Anomaly Products in Different Regions (Unit: mGal)

Region	SIO V33.1 GRA		SWOT_04GRA		DTU21GRA		SDUST2025GRA	
	MEAN	RMS	MEAN	RMS	MEAN	RMS	MEAN	RMS
A	0.62	3.56	0.75	3.35	0.50	3.43	0.55	3.33
B	0.33	4.73	0.35	4.14	0.16	4.13	0.19	3.83
C	-0.49	3.77	-0.47	3.40	-0.60	3.39	-0.54	3.27
D	0.17	2.64	0.03	2.41	0.18	2.60	0.17	2.37

Table 7 shows that, in all four representative regions, SDUST2025GRA yields lower RMS differences against the shipborne gravity anomaly data than the other three comparison products. This indicates good validation accuracy under different seafloor topographic settings. In Region B, where seamounts and trenches are densely distributed, the RMS of SDUST2025GRA is lower than that of SIO V33.1 GRA by 0.90 mGal. The reductions relative to SWOT_04GRA and DTU21GRA are 0.31 mGal and 0.30 mGal, respectively. In Region C, which is mainly characterized by a seamount chain, the RMS is reduced by 0.50 mGal relative to SIO V33.1 GRA. The corresponding reductions relative to SWOT_04GRA and DTU21GRA are 0.13 mGal and 0.12 mGal, respectively. These results indicate that SDUST2025GRA agrees better with shipborne observations in regions with pronounced seafloor relief, such as trenches and seamounts. SDUST2025GRA is derived from the SDUST2025DOV dataset, which is directly determined from 2D SWOT/KaRIn wide-swath altimetry observations using local geoid fitting. The validation results in Regions B and C suggest that the 2D spatial information provided by SWOT/KaRIn observations is beneficial for representing gravity field variations associated with complex seafloor relief. In Regions A and D, SDUST2025GRA also achieves the lowest RMS values. However, its improvements over SWOT_04GRA are only 0.02 mGal and 0.04 mGal, respectively, indicating relatively limited accuracy gains. This suggests that, in regions with relatively simple topographic variations or weak spatial variability of the gravity field, the two SWOT-based products perform similarly. The differences in their validation results are less pronounced than those observed in regions with complex seafloor topography.

The differences between the four gravity anomaly products and the shipborne

https://doi.org/10.5194/essd-2026-712
Preprint. Discussion started: 21 September 2026

Open Access Earth System Science Data Discussions

gravity anomaly data are further analyzed under different water-depth conditions, and the results are shown in Fig. 8. As shown in the figure, SDUST2025GRA generally exhibits lower STD values of the differences over most water-depth intervals. Compared with SWOT_04GRA, SDUST2025GRA shows different performance across water-depth intervals. At depths shallower than approximately 2100 m, SDUST2025GRA achieves lower STD values than SWOT_04GRA, indicating better accuracy in shallow-water regions and shelf-break transition zones. Within the depth range of approximately 2100-3800 m, SWOT_04GRA shows slightly lower STD values than SDUST2025GRA, suggesting better agreement with shipborne observations in this interval. However, at depths greater than approximately 3800 m, SDUST2025GRA again outperforms SWOT_04GRA. In ultra-deep regions with water depths exceeding approximately 6500 m, the STD values of all products show certain fluctuations, with increased errors observed for some products. This may be related to the fact that ultra-deep regions are commonly associated with trenches and tectonic boundaries, where gravity field variations are relatively strong. In addition, the number and spatial distribution of shipborne gravity anomaly observations in these regions may be insufficiently uniform, making the statistical results more susceptible to local topographic characteristics and sample distribution.

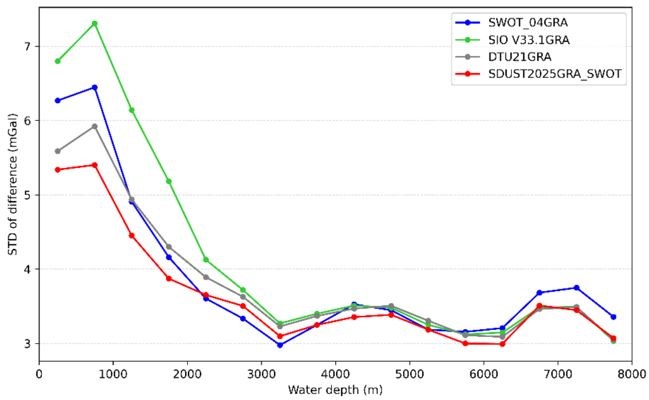

Figure 8. STD Values of Differences Between Gravity Anomaly Models and Shipborne Gravity Anomaly Data under Different Water-Depth Conditions

5 Data availability

The global marine DOV and gravity anomaly datasets, SDUST2025DOV_SWOT and SDUST2025GRA_SWOT, are available at https://doi.org/10.5281/zenodo.21408557 (Zhang et al., 2026). The

https://doi.org/10.5194/essd-2026-712
Preprint. Discussion started: 21 September 2026

SDUST2025DOV_SWOT dataset contains longitude, latitude, and DOV components, whereas the SDUST2025GRA_SWOT dataset contains longitude, latitude, and gravity anomaly data.

6 Conclusions

When deriving marine DOVs from altimetry data, the remove-restore technique is commonly used. Consequently, the long-wavelength components of the resulting DOVs depend to some extent on the adopted reference gravity field model. SWOT/KaRIn wide-swath altimetry provides 2D SSH observations, offering a new data basis for constructing high-resolution marine DOV and gravity anomaly datasets. In this study, a global marine DOV dataset, SDUST2025DOV, is generated from SWOT/KaRIn wide-swath altimetry using a local geoid fitting approach that does not rely on the conventional RCR strategy. The corresponding global marine gravity anomaly dataset, SDUST2025GRA, is further derived from SDUST2025DOV.

To assess the quality of SDUST2025DOV, comparisons are conducted with two established global marine DOV products, SIO V33.1DOV and SWOT_04DOV. Over the global ocean domain spanning longitudes from 0° to 360° and latitudes from -77.6° to 77.6°, the STDs of the meridian component differences are both 1.41 μrad. For the prime vertical component, the corresponding STDs are 1.63 μrad against SIO V33.1DOV and 1.56 μrad against SWOT_04DOV. Overall, SDUST2025DOV shows good agreement with both reference products in the meridian and prime vertical components, demonstrating the good quality of the SDUST2025DOV dataset. The agreement between SDUST2025DOV and SWOT_04DOV is better for the prime vertical component than that between SDUST2025DOV and SIO V33.1DOV. A possible explanation is that both SDUST2025DOV and SWOT_04DOV are derived using SWOT/KaRIn wide-swath altimetry data. This result suggests that the 2D observations provided by SWOT/KaRIn can improve the representation of the prime vertical component compared with conventional nadir altimetry. Typical regions with different seafloor topographic settings are also selected to analyze the correlations between the DOV products and seafloor topographic slopes. The results show that DOV products derived from SWOT/KaRIn wide-swath altimetry exhibit higher correlations with seafloor topographic slopes at short wavelengths than SIO V33.1DOV. This indicates that 2D SWOT/KaRIn observations are beneficial for representing medium and short wavelength gravity field signals associated with seafloor topography.

https://doi.org/10.5194/essd-2026-712
Preprint. Discussion started: 21 September 2026

However, the correlation between SDUST2025DOV and seafloor topographic slope is slightly lower than that of SWOT_04DOV. This difference may be related to the number of SWOT/KaRIn cycles used and the product versions adopted by the two datasets. SWOT_04DOV is constructed from 42 cycles of SWOT/KaRIn L2 data, whereas SDUST2025DOV uses 33 cycles of L3 data. The L3 product undergoes additional filtering and error processing based on the L2 product. These procedures improve data stability but may smooth part of the high-frequency information. Consequently, SDUST2025DOV shows a slightly weaker correlation with short wavelength seafloor topographic signals than SWOT_04DOV.

To further evaluate the accuracy of the gravity anomaly products, the processed shipborne gravity anomaly data are used as independent validation data. SDUST2025GRA is assessed together with SIO V33.1 GRA, SWOT_04GRA, and DTU21GRA. Over the global ocean domain spanning 0°-360° in longitude and -77.6°-77.6°in latitude, the STD of the differences between SDUST2025GRA and the shipborne gravity anomaly data is 3.82 mGal. The corresponding STD is 3.69 mGal for middle and low latitude regions. For high latitude regions, the STD is 4.98 mGal. These values are lower than those of the other comparison products. The results indicate good agreement between SDUST2025GRA and the independent shipborne gravity anomaly data, demonstrating the good accuracy of the SDUST2025GRA dataset. Since SDUST2025GRA is derived from the SDUST2025DOV dataset, the validation results of the gravity anomaly dataset also provide indirect support for the quality of the SDUST2025DOV dataset. The performance of SDUST2025GRA is further evaluated under different seafloor topographic settings and water-depth conditions. In regions with pronounced relief, such as seamounts and trenches, SDUST2025GRA shows more evident accuracy improvements over the other products. In regions with relatively smooth topography, SDUST2025GRA still achieves the best accuracy, but its improvements over the other products are less pronounced. The water-depth-dependent statistics also show that SDUST2025GRA maintains relatively low STD values over most depth intervals. Its overall performance is better than or comparable to that of the other products. Based on the above results, SDUST2025GRA shows competitive performance compared with existing gravity anomaly products. Together with the SDUST2025DOV dataset, these datasets provide new global marine gravity field data resources for scientific research and related applications.

https://doi.org/10.5194/essd-2026-712
Preprint. Discussion started: 21 September 2026

Author contributions.

HZ and JG designed the research and developed the algorithm. SY downloaded altimeter data and other data. SB carried out the experimental results and wrote the manuscript. YJ and XL gave related comments for this work.

Competing interests.

The contact author has declared that none of the authors has any competing interests.

Disclaimer.

Publisher's note: Copernicus Publications maintains neutrality regarding jurisdictional claims in published maps and institutional affiliations.

Acknowledgements.

We thank AVISO for providing KaRIn altimetry data from the NASA/CNES SWOT mission. We are grateful to CMEMS for making the MIOST data available and to ICGEM for supplying the reference gravity field models. We also acknowledge DTU for providing the DTU21GRA model and SIO for releasing the SWOT_04 and SIO V33.1 models. Our appreciation is extended to NCEI and JAMSTEC for sharing the shipborne gravity anomaly data. Finally, we acknowledge the Generic Mapping Tools (GMT) project and its contributors for their support in data processing and visualization.

Financial support.

This work is supported by the National Natural Science Foundation of China, under grant numbers: 42430101 and 42274006.

References

Allain, V., Kerandel, J., Andréfouët, S., Magron, F., Clark, M., Kirby, D., and Muller-Karger, F.: Enhanced seamount location database for the western and central Pacific Ocean: Screening and cross-checking of 20 existing datasets, Deep-Sea Res. Pt. I, 55, 1035-1047, https://doi.org/10.1016/j.dsr.2008.04.004, 2008.

Andersen, O. B., Knudsen, P., Ludwigsen, C., Rose, S. K., and Abulaitijiang, A.: The DTU21 global marine gravity field based on existing altimetric geodetic missions and outlook towards the use of SWOT, XXVIII General Assembly of the International Union of Geodesy and Geophysics, https://doi.org/10.57757/IUGG23-1278, 2023.

Andersen, O. B., Zhang, S., Sandwell, D. T., Dibarboure, G., Smith, W.H.F., and Abulaitijiang, A.: The unique role of the Jason geodetic missions for high resolution gravity field and mean sea surface modelling, Remote Sens., 13, 646, https://doi.org/10.3390/rs13040646, 2021.

AVISO/DUACS: SWOT Level-3 KaRIn low rate SSH unsmoothed (v2.0.1). CNES [Data set], https://doi.org/10.24400/527896/A01-2024.003, 2024.

https://doi.org/10.5194/essd-2026-712
Preprint. Discussion started: 21 September 2026

Chao, N., Wang, S., Ouyang, G., Hwang, C., Jin, T., Zhu, C., Abulaitijiang, A., Zhang, S., Yue, L., Chen, G., and Zhang, Y.: An improved triple collocation-based integration of multiple gravity anomaly grids from satellite altimetry: Contribution of ICESat-2, Remote Sens. Environ., 292, 113582, https://doi.org/10.1016/j.rse.2023.113582, 2023.

Che, D., Li, H., Zhang, S., and Ma, B.: Calculation of deflection of vertical and gravity anomalies over the south China sea derived from ICESat-2 data, Front. Earth Sci., 9: 670256, https://doi.org/10.3389/feart.2021.670256, 2021.

Chen, X., Zhang, S., Andersen, O. B., and Jia, Y.: Along-Track Marine geoid resolution enhancement with SWOT, Earth Space Sci., 12, e2024EA003893, https://doi.org/10.1029/2024EA003893, 2025.

de Vargas, M. R., Mohn, G., Tugend, J., Kusznir, N., Lin, A., and Lin, L.: Tectonostratigraphic evolution of the northeast south China sea rifted margin: From Mesozoic orogeny to present, Earth Sci. Rev., 278, 105501, https://doi.org/10.1016/j.earscirev.2026.105501, 2026.

Dibarboure, G., Anadon, C., Briol, F., Cadier, E., Chevrier, R., Delepoulle, A., Faugère, Y., Laloue, A., Morrow, R., Picot, N., Prandi, P., Pujol, M., Raynal, M., Tréboutte, A., and Ubelmann, C.: Blending 2D topography images from the Surface Water and Ocean Topography (SWOT) mission into the altimeter constellation with the Level-3 multi-mission Data Unification and Altimeter Combination System (DUACS), Ocean Sci., 21, 283-323, https://doi.org/10.5194/os-21-283-2025, 2025.

Guo, H., Wan, X., and Wang, H.: Validation of just-released SWOT L2 KaRIn beta prevalidated data based on restore the marine gravity field and its application, IEEE J. Sel. Top. Appl. Earth Obs. Remote Sens., 2024, 17, 7878-7887, https://doi.org/10.1109/JSTARS.2024.3382976, 2024.

Guo, H., Wan, X., and Wu, X.: Deriving deflection of the vertical and gravity anomaly from SWOT/KaRIn data using an optimized discretization method, Remote Sens., 18(9): 1360, https://doi.org/10.3390/rs18091360, 2026.

Han, Y., Qin, F., Li, K., Xiao, Y., and Zhu, T.: A topography-constrained marine gravity field modeling method for gravity matching-aided navigation, IEEE Sens. J., 26, 19121-19133, https://doi.org/10.1109/JSEN.2026.3691309, 2026.

Hwang, C.: Inverse Vening Meinesz formula and deflection-geoid formula: Applications to the predictions of gravity and geoid over the South China Sea, J. Geod., 72: 304-312, https://doi.org/10.1007/s001900050169, 1998.

Hwang, C., Kao, E., and Parsons, B.: Global derivation of marine gravity anomalies from Seasat, Geosat, ERS-1 and TOPEX/POSEIDON altimeter data, Geophys. J. Int., 134, 449-459, https://doi.org/10.1111/j.1365-246X.1998.tb07139.x, 1998.

Hwang, C., and Parsons, B.: Gravity anomalies derived from Seasat, Geosat, ERS-1 and TOPEX/POSEIDON altimetry and ship gravity: A case study over the Reykjanes Ridge, Geophys. J. Int., 122, 551-568, https://doi.org/10.1111/j.1365-246X.1995.tb07013.x, 1995.

Hwang, C., and Yu, D.: Transforming coastal mapping from space, Science, 386, 1222-1223, https://doi.org/10.1126/science.adu0697, 2024.

https://doi.org/10.5194/essd-2026-712
Preprint. Discussion started: 21 September 2026

Ji, H., Guo, J., Zhu, C., Yuan, J., Liu, X., and Li, G.: On deflections of vertical determined from HY-2A/GM altimetry data in the Bay of Bengal, IEEE J. Sel. Top. Appl. Earth Obs. Remote Sens., 14, 12048-12060, https://doi.org/10.1109/JSTARS.2021.3129273, 2021.

Jin, T., Zhou, M., Zhang, H., Li, J., Jiang, W., Zhang, S., and Hu, M.: Analysis of vertical deflections determined from one cycle of simulated SWOT wide-swath altimeter data, J. Geod., 96, 30, https://doi.org/10.1007/s00190-022-01619-8, 2022.

Laloue, A., Schaeffer, P., Pujol, M., Veillard, P., Andersen, O., Sandwell, D., Delepoulle, A., Dibarboure, G., and Faugère, Y.: Merging recent mean sea surface into a 2023 hybrid model (From Scripps, DTU, CLS, and CNES), Earth Space Sci., 12, e2024EA003836, https://doi.org/10.1029/2024EA003836, 2025.

Li, Y., Zhou, J., Li, J., Li, N., Zhu, F., and Sun, H.: Global marine gravity from 27 cycles of SWOT satellite data: Accuracy and spatial resolution evaluation, J. Geod., 99, 51, https://doi.org/10.1007/s00190-025-01972-4, 2025.

Li, Z., Guo, J., Hwang, C., Yu, D., Zhang, H., Sun, H., and Liu, X.: Tailored method for optimizing deflection of the vertical model using multidirectional geoid gradients from SWOT/KaRIn observations, Geophys. J. Int., 244, ggaf484, https://doi.org/10.1093/gji/ggaf484, 2026.

Li, Z., Guo, J., Zhu, C., Liu, X., Hwang, C., Lebedev, S., Chang, X., Soloviev, A., and Sun, H.: The SDUST2022GRA global marine gravity anomalies recovered from radar and laser altimeter data: contribution of ICESat-2 laser altimetry, Earth Syst. Sci. Data, 16, 4119-4135, https://doi.org/10.5194/essd-16-4119-2024, 2024.

Liang, W., Li, J., Xu, X., Zhang, S., and Zhao, Y.: A high-resolution Earth's gravity field model SGG-UGM-2 from GOCE, GRACE, Satellite Altimetry, and EGM2008. Engineering, 6, 860-878, https://doi.org/10.1016/j.eng.2020.05.008, 2020.

Ling, Z., Zhao, L., Zhang, T., Zhai, G., and Yang, F.: Comparison of marine gravity measurements from shipborne and satellite altimetry in the Arctic Ocean, Remote Sens., 14, 41, https://doi.org/10.3390/rs14010041, 2021.

Marks, K.M., and Smith, W.H.F.: Detecting small seamounts in AltiKa repeat cycle data, Mar. Geophys. Res., 37, 349-359, https://doi.org/10.1007/s11001-016-9293-0, 2016.

Peng, H., Liu, X., Li, Z., Wei, X., Fan, X., and Guo, J.: Optimized estimation of marine deflection of the vertical from multibeam laser altimeter data of ICESat-2, Geophys. J. Int., 239, 455-466, https://doi.org/10.1093/gji/ggae280, 2024.

Salajegheh, F., Deng, X., Andersen, O., Coleman, R., and Khaki, M.: SWOT global bathymetry modeling using deep neural networks trained on multiple geophysical features, Earth Space Sci., 12, e2025EA004545, https://doi.org/10.1029/2025EA004545, 2025.

Sandwell, D., Harper, H., Tozer, B., and Smith, W.H.F.: Gravity field recovery from geodetic altimeter missions, Adv. Space Res., 68, 1059-1072, https://doi.org/10.1016/j.asr.2019.09.011, 2021.

Sdrolias, M., and Müller, R.: Controls on back-arc basin formation. Geochem, Geophys. Geosyst., 7, Q04001, https://doi.org/10.1029/2005GC001090, 2006.

https://doi.org/10.5194/essd-2026-712
Preprint. Discussion started: 21 September 2026

Sandwell, D., Müller, R., Smith, W.H.F., Garcia, E., and Francis, R.: New global marine gravity model from CryoSat-2 and Jason-1 reveals buried tectonic structure, Science, 346, 65-67, https://doi.org/10.1126/science.1258213, 2014.

SSALTO/DUACS: Gridded sea level height and geostrophic velocities computed with SWOT Level-3 products using both KaRIn and nadir instruments, CMEMS [Data set], https://doi.org/10.48670/moi-00147, 2025.

Sun, M., Feng, W., An, D., Chen, X., Yang, M., and Zhong, M.: Preliminary results of marine gravity anomaly and bathymetry from SWOT wide-swath altimeter data, IEEE J. Sel. Top. Appl. Earth Obs. Remote Sens., 18, 18107-18116, https://doi.org/10.1109/JSTARS.2025.3588419, 2025.

Wan, X., Annan, R.F., Jin, S., and Gong, X.: Vertical deflections and gravity disturbances derived from HY-2A data, Remote Sens., 12, 2287, https://doi.org/10.3390/rs12142287, 2020.

Wan, X., Hao, R., Jia, Y., Wu, X., Wang, Y., and Feng, L.: Global marine gravity anomalies from multi-satellite altimeter data, Earth Planets Space, 74, 165, https://doi.org/10.1186/s40623-022-01720-4, 2022.

Wang, J., Xu, Y., Zhang, Q., Wang, Y., Zhu, C., and Xu, H.: Improving high-frequency marine gravity anomaly recovery: The efficacy of SWOT wide-swath altimetry, IEEE Geosci. Remote Sens. Lett., 21, 7505905, https://doi.org/10.1109/LGRS.2024.3431694, 2024.

Witter, R., Briggs, R., Dura, T., Engelhart, S., and Nelson, A.: Seismic sources in the Aleutian cradle of tsunamis, Eos, 103, https://doi.org/10.1029/2022EO220464, 2022.

Wu, Y., Andersen, O., Abulaitijiang, A., Luo, Z., Wang, H., and He, X.: High-resolution quasi-geoid recovery over coastal zone by using airborne gravity gradient data, IEEE Trans. Geosci. Remote Sens., 63, 4209121. https://doi.org/10.1109/TGRS.2025.3588586, 2025.

Xiao, Y., Jin, T., Li, J., Hu, J., Zhou, M., and Li, X.: An improved multidirectional retrieval method of vertical deflection components from SWOT wide-swath data. IEEE Trans, Geosci. Remote Sens., 64, 4207013, https://doi.org/10.1109/TGRS.2026.3688869, 2026.

Ya, S., Liu, X., Li, Z., Zhou, R., Bian, S., and Guo, J.: Data interpolation of SWOT/KaRIn blank for modelling marine vertical gradient of gravity anomaly, Geophys. J. Int., 245, ggag039, https://doi.org/10.1093/gji/ggag039, 2026.

Yu, D., and Hwang, C.: Optimized processing of SWOT fast-sampling data for marine gravity recovery: Lessons for the 21-day science phase, Remote Sens. Environ., 328, 114903, https://doi.org/10.1016/j.rse.2025.114903, 2025.

Yu, Y., Sandwell, D., and Dibarboure, G.: Abyssal marine tectonics from the SWOT mission, Science, 386, 1251-1256, https://doi.org/10.1126/science.ads4472, 2024.

Yu, Y., Sandwell, D., Gille, S., and Bôas, A.: Assessment of ICESat-2 for the recovery of ocean topography, Geophys. J. Int., 226, 456-467, https://doi.org/10.1093/gji/ggab084, 2021.

Zhang, S., Chen, X., Zhou, R., and Jia, Y.: NSOAS24: a new global marine gravity

https://doi.org/10.5194/essd-2026-712
Preprint. Discussion started: 21 September 2026

Open Access Earth System Science Data Discussions

model derived from multi-satellite sea surface slopes, Geosci. Model Dev., 18, 1221–1239, https://doi.org/10.5194/gmd-18-1221-2025, 2025.

Zhang, S., Sandwell, D., Jin, T., and Li, D.: Inversion of marine gravity anomalies over southeastern China seas from multi-satellite altimeter vertical deflections, J. Appl. Geophys., 137, 128-137, https://doi.org/10.1016/j.jappgeo.2016.12.014, 2017.

Zhu, C., Guo, J., Gao, J. Liu, X., Hwang, C., Yu, S., Yuan, J., Ji, B., and Guan, B.: Marine gravity determined from multi-satellite GM/ERM altimeter data over the South China Sea: SCSGA V1.0, J. Geod., 94, 50, https://doi.org/10.1007/s00190-020-01378-4, 2020.

Zhang, H., Guo, J., Ya, S., Bian, S., Jia, Y., and Liu, X.: Global marine vertical deflection model SDUST2025DOV_SWOT and gravity anomaly model SDUST2025GRA_SWOT derived from SWOT/KaRIn data using local geoid fitting method [Dataset]. Zenodo. https://doi.org/10.5281/zenodo.21408557, 2026.

Zhu, C., Guo, J., Ya, S., Li, W., Gao, J., and Qiu, L.: Moving geoid gradient method for high-precision and high-resolution gravity recovery from SWOT wide-swath data, IEEE Trans. Geosci. Remote Sens., 63, 4205613, https://doi.org/10.1109/TGRS.2025.3563949, 2025.

Zhu, C., Guo, J., Yuan, J., Li, Z., Liu, X., and Gao, J.: SDUST2021GRA: global marine gravity anomaly model recovered from Ka-band and Ku-band satellite altimeter data, Earth Syst. Sci. Data, 14, 4589–4606, https://doi.org/10.5194/essd-14-4589-2022, 2022.

Zhu, T., Qin, F., Li, Z., Li, A., Li, K., Qian, L., and Han, Y.: A novel matching algorithm based on SE2(3) in local-level frame for underwater gravity-aided navigation, Measurement, 281, 122032, https://doi.org/10.1016/j.measurement.2026.122032, 2026.

Zingerle, P., Pail, R., Gruber, T., and Oikonomidou, X.: The combined global gravity field model XGM2019e, J. Geod., 94, 66, https://doi.org/10.1007/s00190-020-01398-0, 2020.